Complementary Metal–Oxide–Semiconductor Micro-Electro-Mechanical-System Reconfigurable Cantilever Resonator with Multiple Electrostatic Electrodes

2010 Jpn. J. Appl. Phys. 49 116501

(http://iopscience.iop.org/1347-4065/49/11R/116501)

Complementary Metal–Oxide–Semiconductor Micro-Electro-Mechanical-System Reconfigurable Cantilever Resonator with Multiple Electrostatic Electrodes

Li-Jung Shieh[1] and Jin-Chern Chiou[1,2,3*]

[1]*Institute of Electrical Control Engineering, National Chiao Tung University, Hsinchu 30010, Taiwan, R.O.C.*
[2]*Department of Electrical Engineering, National Chiao Tung University, Hsinchu 30010, Taiwan, R.O.C.*
[3]*School of Medicine, China Medical University, Taichung 40402, Taiwan, R.O.C.*

Received February 3, 2010; revised August 2, 2010; accepted August 3, 2010; published online November 22, 2010

In this paper, we present a prestress vertical comb drive resonator with a frequency tuning capability. The resonator consists of three sets of comb fingers, which act as driving electrodes. The comb fingers are fabricated along with a composite beam. One end of the composite beam is clamped to the anchor, whereas the other end is elevated vertically by the residual stress. A clamped force, which is formed by a DC voltage, is utilized to restrain the vibration of the composite beam. By applying a DC clamped voltage and a driving voltage in different electrodes, the resonator exhibits different frequency responses. The device is fabricated through a 0.35 μm complementary metal–oxide–semiconductor (CMOS) process with a post-CMOS micromachining process. Experimental results indicate that the initial resonant frequency of the device is 18.6 kHz, and the maximum frequency tuning range up to 28.5% is obtained. The resonator device can recover its original frequency without causing any structural damage.

DOI: 10.1143/JJAP.49.116501

1. Introduction

Microresonators with electrostatic actuation have been employed in various microsystems, such as resonant accelerometers,[1–3] microelectromechanical filters,[4,5] and chemical sensors.[6,7] The main benefit of electrostatic excitation is its characteristic low power consumption. Recently, various electrostatic actuation methods, such as those using parallel-plate and comb drive structures, have been developed. Electrostatic comb actuators are developed to suppress the occurrence of a vertical pull-in phenomenon in a vertical resonator with a parallel plate electrostatic actuator.[8,9] The comb-drive structure also has an advantage over parallel-plates, in that the electrostatic force is independent of the displacement of the actuator.

In most resonators, resonant frequency is an important parameter in measurement. However, it tends to deviate from the designed value owing to micromachining process variations, the operating environment, as well as aging and contamination.[9–12] Therefore, the resonant frequency of a microresonator must be tuned after fabrication for numerous applications.[13,14] Various frequency tuning methods have been demonstrated; they can be grouped into two major categories, namely, active tuning and passive tuning. Active tuning schemes include electrostatic and electrothermal tuning. Electrostatic tuning methods generally apply a tuning voltage to alter the stiffness of capacitive structures.[15–19] Electrothermal tuning changes the thermal stress of microstructures with an input power.[20–23] Inducing stress in a device also changes the effective stiffness of the device. Active tuning methods do not permanently modify or damage structures. They are suitable for real time tuning when environmental changes alter the frequency of the resonator. In contrast, passive tuning methods usually make permanent changes by dimensional trimming. In other words, passive tuning is none other than mass tuning. Previous investigations have been demonstrated using many tools for passive tuning, such as those for laser trimming,[24,25] a focused ion beam (FIB),[26,27] deposition,[28,29] and ion milling.[30] These instruments usually need a high processing temperature and are costly.

In this work, we present a vertical electrostatic resonator with a frequency tuning capability and a multiple-electrode configuration. The resonant frequency of this resonator can be tuned by changing the stiffness by driving with different electrodes. Complementary metal–oxide–semiconductor micro-electro-mechanical-system (CMOS–MEMS) technology is used for fabrication. The following sections present the operating principle, theoretical analysis and simulation, fabrication process, and experimental results.

2. Operating Principle

The electrostatic actuation method for the developed resonator is based on a prestress comb-drive structure.[31] Figure 1 schematically depicts a resonator with different driving states. The resonator consists of an anchor, a composite beam, and a set of comb fingers. These comb fingers, designed along the composite beam, acted as the movable and fixed comb fingers. One end of the composite beam is clamped to the anchor and the other end is elevated due to the residual stress between the two deposited materials, as shown in Fig. 1(a). When a voltage, V, is applied between the movable and fixed comb fingers, the movable composite beam can be pulled downward to the substrate using the electrostatic force induced by the fringe effect, as shown in Fig. 1(b). The taper-like distances between each movable and fixed comb are obtained from the free end to the fixed end, on the basis of the curved-up shape of the composite beam. In the actuating mechanisms, the movable comb fingers that are close to the anchor provide the main actuation force. As the actuation progresses, these movable comb fingers will be pulled down accordingly. With the driving voltage, the vertical displacement of the free end of the resonator increases. Compared with the parallel-plate electrostatic actuator, the vertical comb drive exhibits no pull-in and hysteresis phenomenon. Notably, the electrostatic force is constrained when the movable comb finger is close to the fixed comb finger, independently of input driving voltage, as shown in Fig. 1(c). If the fixed fingers are divided into several sets as multiple fixed electrodes, the resonator can be driven under various conditions. Figure 2 illustrates a resonator with three sets of driving electrodes. By applying different voltage signals in different fixed

*E-mail address: chiou@mail.nctu.edu.tw

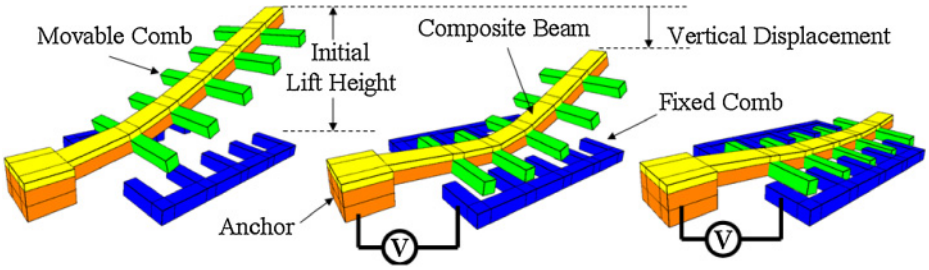

Fig. 1. (Color online) Resonator at different driving states: (a) initial state, (b) bias voltage state, and (c) critical bias voltage state.

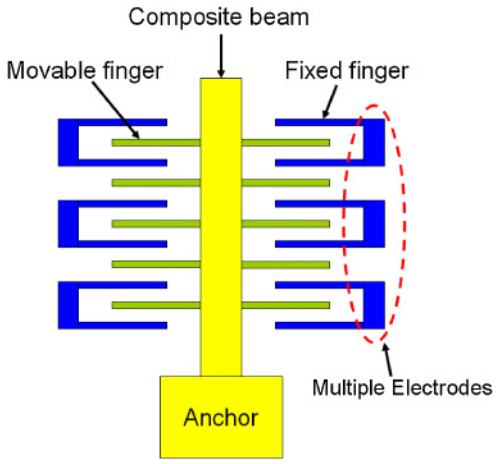

Fig. 2. (Color online) Architecture of the proposed multiple-electrostatic-electrode resonator.

electrodes, the resonator will exhibit dissimilar frequency responses. For example, in the case of an additional DC voltage applied to one of the three fixed electrodes while the others are driven with the sinusoidal wave voltage, the frequency response will differ from that in all fixed electrodes provided with the same sinusoidal driving voltage.

3. Theoretical Analysis and Finite Element Method (FEM) Simulation

3.1 Resonant frequency analysis

The resonant frequency of a homogeneous cantilever beam with a uniform cross section is defined as[32)]

$$f_n = \frac{\lambda_n^2}{2\pi L^2}\sqrt{\frac{EI}{\rho A}}, \tag{1}$$

where λ_n is a dimensionless parameter, which is determined by boundary conditions. λ_n for the first three modes of a cantilever beam is shown in Table I.[32–35)] L, E, I, ρ, and A are the length, Young's modulus, moment of inertia about the neutral axis, density, and cross-sectional area of the cantilever beam, respectively. Composite beams may be analyzed using the same theory as that for ordinary beams, since the assumption that plane cross sections remain plane after bending is valid in pure bending, independently of the material used.[36)] Therefore, the natural frequency of a composite beam can be approximated as

Table I. λ_n for the first three modes of a cantilever beam.

n	λ_n
1	1.875
2	4.694
3	7.855

$$f_n = \frac{\lambda_n^2}{2\pi L^2}\sqrt{\frac{\sum_{i=1}^{N} E_i I_i}{\bar{\rho} A_s}}, \tag{2}$$

where N is the number of layers in the composite beam, E_i and I_i are respectively the Young's modulus and moment of inertia of each layer, A_s is the sum of the cross-sectional area of each layer, and $\bar{\rho}$ is the average specific mass density of the composite beam, which is given by

$$\bar{\rho} = \frac{\sum_{i=1}^{N} \rho_i t_i}{\sum_{i=1}^{N} t_i}, \tag{3}$$

where ρ and t are the density and thickness of each layer, respectively.

The moment of inertia of each layer is defined by[36)]

$$I_i = \frac{bt_i^3}{12} + bt_i d_i^2, \tag{4}$$

where b is the width of the composite beam, t_i is the thickness of each layer, and d_i is the distance between the centroid of the composite beam and the neutral axis of each layer. Figure 3 illustrates the structure and dimensions of the proposed resonator. The thickness and material property of each layer in the CMOS process are obtained from the National Chip Implementation Center.[37)] Therefore, the theoretical resonant frequency of the resonator is calculated as 17 kHz using eq. (2).

3.2 Frequency tuning analysis

For frequency tuning, the system can be described using the energy method. In general, the electrostatic force of a comb drive actuator can be expressed as

$$F_e = \frac{\partial U_e}{\partial z} = \frac{1}{2} N \frac{\partial C}{\partial z} V^2, \tag{5}$$

where U_e is the electrostatic energy of the comb drive actuator, N is the number of comb fingers, V is the applied

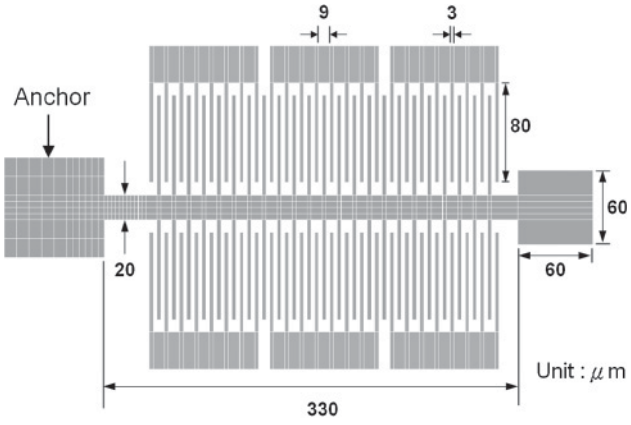

Fig. 3. Dimensions of the proposed resonator.

voltage, and $\partial C/\partial z$ is the gradient of capacitance of comb fingers in the z-direction.

In addition, the mechanical strain energy of the beam is given by

$$U_m = \frac{1}{2}kz^2, \tag{6}$$

where k and z are the unstrained spring constant and deflection of the beam, respectively. The work done by electrostatic force is stored in the device in the form of elastic strain energy. The total potential energy (U) stored in the system is given by

$$U = \frac{1}{2}k_{\text{eff}}z^2 = U_m - U_e, \tag{7}$$

where k_{eff} is the overall effective spring constant. By considering the second derivative of eq. (7), an expression of k_{eff} is obtained as

$$k_{\text{eff}} = k - \frac{1}{2}N\frac{\partial^2 C}{\partial z^2}V^2. \tag{8}$$

Thus, the resonant frequency changes with k_{eff} and can be expressed as

$$f_{\text{tun}} \approx \frac{1}{2\pi}\sqrt{\frac{k_{\text{eff}}}{m_{\text{eq}}}}, \tag{9}$$

where m_{eq} is the equivalent mass of the resonator. By calculating the difference between eqs. (2) and (9), the frequency variation induced by the tuning voltage can be calculated. For instance, an 8% frequency variation is obtained when a tuning voltage of 50 V is applied to the device.

3.3 FEM mode simulation

To understand the resonant characteristics of the resonator, a FEM simulator, IntelliSuite®, is used to calculate the resonant frequency and the corresponding mode shape. The resonator consist of a $330 \times 20\,\mu m^2$ composite beam that is fixed to an anchor structure with 23 movable comb fingers orthogonally mounted on the composite beam, and 24 fixed comb fingers are mounted on the silicon substrate. The dimensions of the comb finger are $80 \times 3\,\mu m^2$, and the overlap length is 70 μm. A $60 \times 60\,\mu m^2$ plate at the free end of the composite beam is used as a sensing area for sensor application in the future. Therefore, the total resonator length is 390 μm. Note that in the present FEM simulations, we solely require movable comb and composite beam to calculate the resonant frequencies. Table II shows the simulation results of the proposed resonator. In the first mode, the resonator bends in the vertical direction and the resonant frequency is 19.7 kHz. The second mode is the yaw motion, and attention must be paid to avoid shorting due to the contact between the movable and fixed comb fingers. In the third mode, the resonator vibrates in the roll motion. These simulation results can be used as the reference data in experimental measurements.

Table II. (Color online) Mode shape of the resonator.

Mode	Frequency (Hz)	Motion	Solid mode shape
1st	19729	Pitch	
2nd	57252	Yaw	
3rd	84678	Roll	

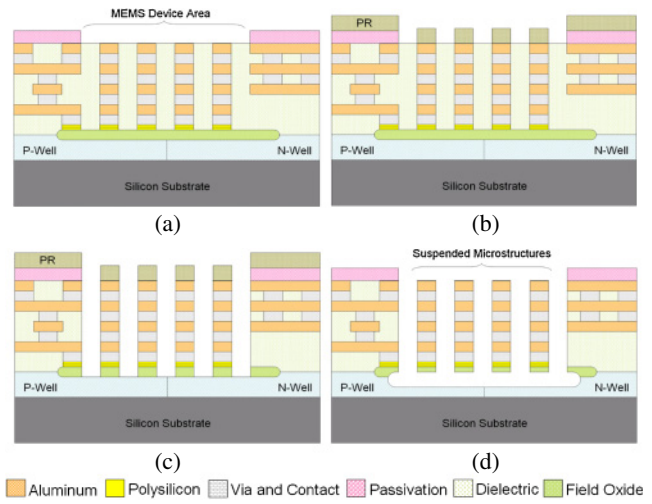

Fig. 4. (Color online) Process flow: (a) completion of CMOS process, (b) patterning a PR mask to protect unnecessary etched regions, (c) etching silicon dioxide by anisotropic RIE, and (d) etching silicon substrate to release suspended microstructure and remove the PR.

4. Fabrication

To fabricate the resonator device, the Taiwan Semiconductor Manufacturing Company (TSMC) standard 0.35 μm double polysilicon quadruple metal (2P4M) CMOS process is employed, followed by the post-CMOS micromachining process.[38] After CMOS fabrication, a two-step dry etching process is used to release the MEMS structures. Figure 4(a) illustrates the cross-sectional view of the MEMS components fabricated through the TSMC 0.35 μm 2P4M CMOS

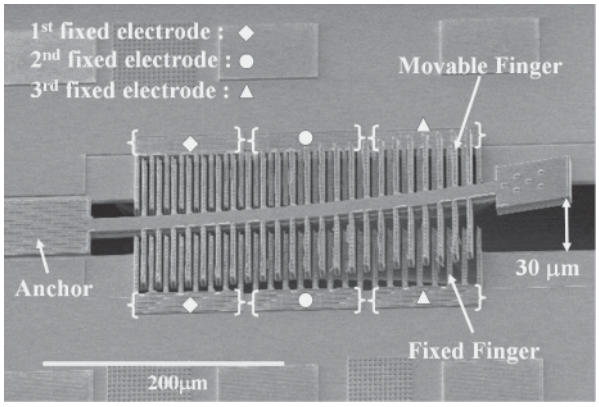

Fig. 5. SEM image of the fabricated resonator device.

process. Before the dry etching steps, a thick photoresist (PR) layer is coated on the chip and patterned, as illustrated in Fig. 4(b). This PR mask is utilized to protect the bonding pads, electronic circuit, and unnecessary etched regions of the MEMS components during dry etching processes. After the PR mask is completed, an anisotropic reactive-ion etching (RIE) process with CHF_3/O_2 plasma is used to define the sidewalls of the device structure and etch the silicon dioxide in the etching holes. Figure 4(c) schematically shows the cross-sectional view of the MEMS device after the anisotropic RIE process. Then, an isotropic RIE with SF_6/O_2 is applied to etch the silicon substrate and release the suspended structures of the MEMS component. Finally, the PR mask is removed and complete the post-CMOS micromachining process, as shown in Fig. 4(d).

Figure 5 displays the resonator device fabricated by the CMOS process and the post-CMOS micromachining. There are three sets of fixed electrodes in the resonator. In order to enhance the electrostatic force, the thickness of the comb fingers must be increased. Hence, the designed comb finger consists of all conductive layers in the CMOS process. Figure 6 illustrates the cross section of the comb fingers. Moreover, the composite beam comprises M3, M4, and all other dielectric layers. The composite beam is bent by the residual stress, as predicted, and the initial tip height at the free end is around 30 μm. By applying a driving voltage between the movable and fixed comb fingers, the resonator can achieve a vertical motion due to the electrostatic force.

5. Measurement and Discussion

To examine the dynamic characteristics of the resonator device, a MEMS motion analyzer (MMA) is used to measure its resonant frequency, as shown in Fig. 7. This instrument uses both bright-field and interference-based illumination modes combined with sophisticated machine vision algorithms to quantify target motions. The resonator is driven by a sinusoidal wave with a voltage offset of 15 V and voltage amplitude of 5 V. First, the original resonant frequency is measured. All fixed electrodes are provided with the same driving voltage. The frequency ranges between 15 and 21 kHz, which agrees with the simulation result. The fundamental resonance frequency mode is measured at 18.6 kHz, which is close to the calculated (17 kHz) and simulated (19.7 kHz) values. The difference among these results is related to fabrication process variations, such as

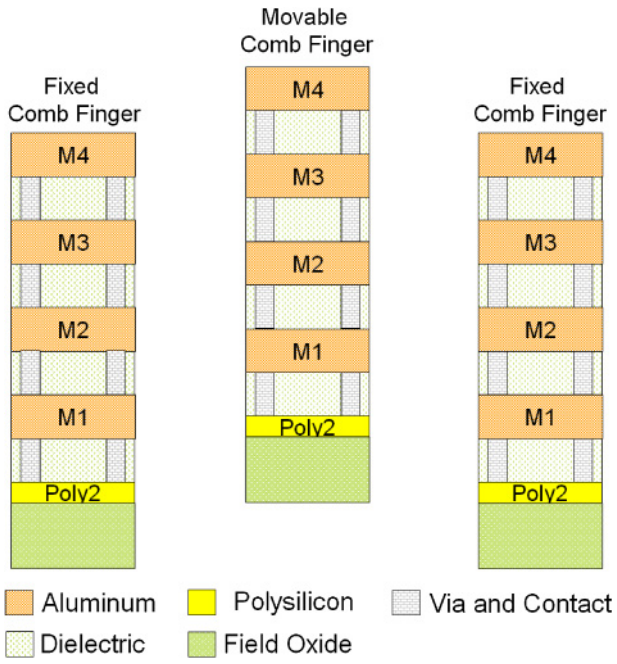

Fig. 6. (Color online) Cross sections of the fixed and movable comb fingers.

Fig. 7. (Color online) MEMS motion analyzer.

those in the thickness of each layer and the undercut of silicon. The quality factor is calculated as 50.

Secondly, a DC voltage is applied to one of the three fixed electrodes while the others are still driven with the sinusoidal wave voltage, as mentioned above. Figures 8–10 show the variations in frequency with different DC voltages applied to the first, second, and third fixed electrodes, respectively. The resonant frequency changes as predicted. The DC voltage applied to a fixed electrode can be treated as a clamped force that restrains the vibration of the composite beam. When a DC voltage of more than 150 V is applied to the first or second fixed electrode, the composite beam corresponding to the DC bias fixed electrode will be pulled downward with a very small vibration. This situation is

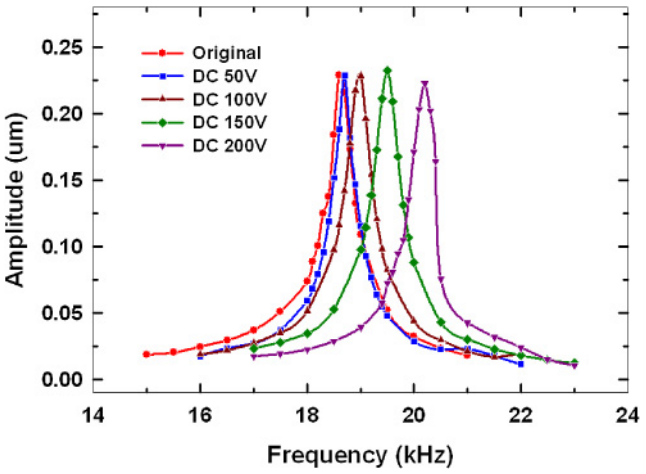

Fig. 8. (Color online) Frequency response of the resonator with DC clamped voltage applied to the first fixed electrode.

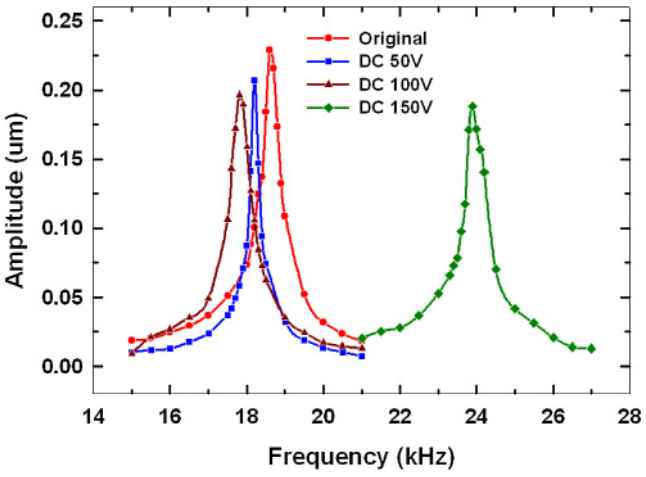

Fig. 9. (Color online) Frequency response of the resonator with DC clamped voltage applied to the second fixed electrode.

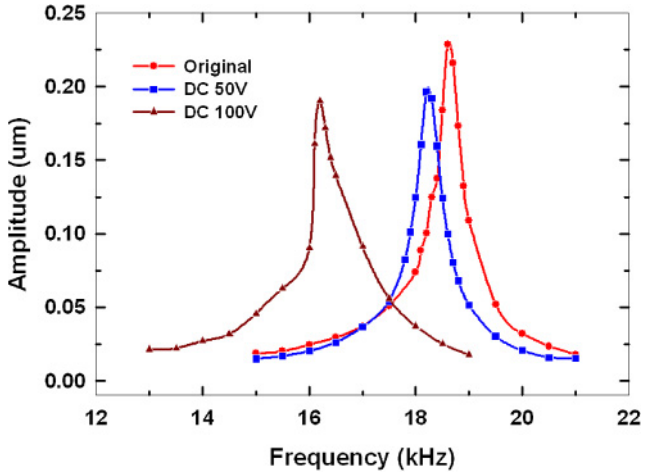

Fig. 10. (Color online) Frequency response of the resonator with DC clamped voltage applied to the third fixed electrode.

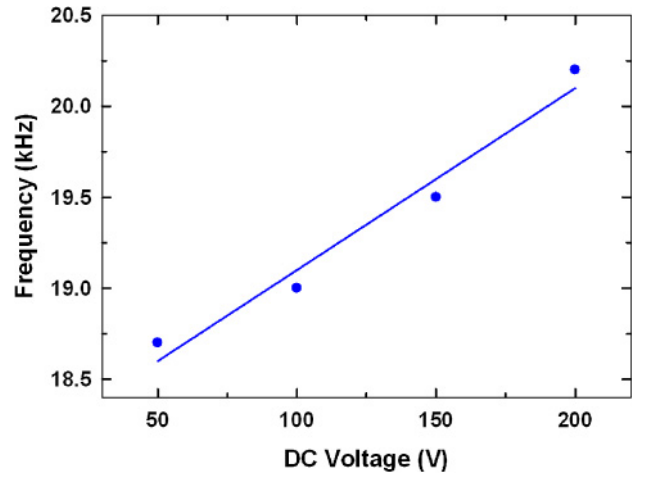

Fig. 11. (Color online) Frequency variations versus DC voltage applied to first fixed electrode.

similar to the case when the fixed end of the composite beam is extended from the original anchor to the fixed electrode where a DC voltage is applied. Therefore, the increases in both stiffness and resonant frequency due to the effective beam length seem to be curtailed. Furthermore, when a DC voltage above 150 V is applied to the third fixed electrode, the configuration of the resonator seems to change from a cantilever beam to a fixed-fixed beam. The stiffness increases substantially, and the resonant frequency cannot be measured with the same driving voltage.

The frequency varies almost linearly when a DC voltage is applied to the first fixed electrode, as shown in Fig. 11. However, a different trend is observed when a DC voltage is applied to the second or third fixed electrode. The resonant frequency decreases when the applied DC voltages are 50 and 100 V. This is due to the fact that the strain energy effect results in a softening spring constant, because the clamped force produced by the DC voltage is not sufficiently large. Nevertheless, when the DC bias voltage is 150 V, the clamped force is sufficiently large for pulling down the composite beam; therefore, the resonant frequency increases substantially similarly to that in the case of a fixed-fixed beam. According to eq. (8), the elastic strain energy contributed by electrostatic force dominates the effective spring constant at low voltages (50 and 100 V), whereas the spring stiffness term (k) dominates at a high voltage (150 V). Moreover, if the DC voltage is applied to both the first and second fixed electrodes, the frequency variation trend is the same as that observed when a DC voltage is applied to the first fixed electrode.

Table III shows a summary of the frequency variations measured with different DC voltages. The maximum frequency variation is up to 28.5% when a DC voltage of 150 V is applied to the second fixed electrode. The resonant frequency of the electrostatic comb drive resonator with a multiple-electrode configuration can clearly be effectively adjusted. The proposed resonator device can also recover its original frequency without causing any structural damage. This approach has potential to become an important tool for the effective frequency tuning of a microresonator device and for use in various applications.

6. Conclusions

A vertical electrostatic resonator with a frequency tuning capability is proposed in this paper. The resonant frequency is adjusted by applying driving voltages to different comb

Table III. Summary of resonant frequency variations.

	Original	DC voltage applied to 1st fixed electrode (V)			
		50	100	150	200
Resonance (kHz)	18.6	18.7	19.0	19.5	20.2
Variation (%)	0	0.5	2.2	4.8	8.6
	Original	DC voltage applied to 2nd fixed electrode (V)			
		50	100	150	200
Resonance (kHz)	18.6	18.2	17.8	23.9	N/A
Variation (%)	0	−2.2	−4.3	28.5	N/A
	Original	DC voltage applied to 3rd fixed electrode (V)			
		50	100	150	200
Resonance (kHz)	18.6	18.2	16.2	N/A	N/A
Variation (%)	0	−2.2	−12.9	N/A	N/A

drive electrodes. The device is implemented using the TSMC 0.35 μm 2P4M CMOS and post-CMOS processes. The design, simulation, and measurement are also presented. The measurement results indicate that the maximum frequency tuning range is up to 28.5%. The excellent frequency tuning capability makes the resonator suitable for many applications, such as a microelectromechanical filter and a chemical sensor.

Acknowledgments

This work was supported by the National Science Council, Taiwan, under Contract Nos. NSC-98-2220-E-009-014 and NSC-98-2218-E-039-001. It was also supported in part by the Department of Health, Taiwan, Clinical Trial and Research Center of Excellence under Contract No. DOH99-TD-B-111-004 and Taiwan Department of Health Cancer Research Center of Excellence under Contract No. DOH99-TD-C-111-005. The authors would also like to thank the National Chip Implementation Center (CIC) for technical support.

1) Y. Omura, Y. Nonomura, and O. Tabata: Proc. 9th Int. Conf. Solid-State Sensors and Actuators, 1997, p. 855.
2) H. Xie and G. K. Fedder: Sens. Actuators A **95** (2002) 212.
3) S. X. P. Su, H. S. Yang, and A. M. Agogino: IEEE Sens. J. **5** (2005) 1214.
4) L. Lin, R. T. Howe, and A. P. Pisano: J. Microelectromech. Syst. **7** (1998) 286.
5) K. Wang, A. C. Wong, and C. T. C. Nguyen: J. Microelectromech. Syst. **9** (2000) 347.
6) S. S. Bedair and G. K. Fedder: Proc. 13th Int. Conf. Solid-State Sensors, Actuators and Microsystems, 2005, p. 2035.
7) C. Ziegler: Anal. Bioanal. Chem. **379** (2004) 946.
8) J. Pons-Nin, A. Rodriguez, and L. M. Castaner: J. Microelectromech. Syst. **11** (2002) 196.
9) W. C. Tang, T. H. Nguyen, and R. T. Howe: Sens. Actuators **20** (1989) 25.
10) A. Pember, J. Smith, and H. Kemhadjian: Appl. Phys. Lett. **66** (1995) 577.
11) Y. K. Yong and J. R. Vig: IEEE Trans. Ultrason. Ferroelectr. Freq. Control **36** (1989) 452.
12) D. Grogg, H. C. Tekin, N. D. Ciressan-Badila, D. Tsamados, M. Mazza, and A. M. Ionescu: J. Microelectromech. Syst. **18** (2009) 466.
13) J. J. Yao and N. C. MacDonald: J. Micromech. Microeng. **5** (1995) 257.
14) Y. Oh, B. Lee, S. Baek, H. Kim, J. Kim, S. Kang, and C. Song: Proc. 10th IEEE Int. Workshop Micro Electro Mechanical Systems, 1997, p. 272.
15) K. B. Lee and Y. H. Cho: Sens. Actuators A **70** (1998) 112.
16) B. E. DeMartini, J. F. Rhoads, K. L. Turner, S. W. Shaw, and J. Moehlis: J. Microelectromech. Syst. **16** (2007) 310.
17) K. B. Lee, A. P. Pisano, and L. Lin: J. Micromech. Microeng. **17** (2007) 557.
18) I. Kozinsky, H. W. Ch. Postma, I. Bargatin, and M. L. Roukes: Appl. Phys. Lett. **88** (2006) 253101.
19) M. Palaniapan and L. Khine: Sens. Actuators A **142** (2008) 203.
20) T. Remtema and L. Lin: Sens. Actuators A **91** (2001) 326.
21) R. R. A. Syms: J. Microelectromech. Syst. **7** (1998) 164.
22) S. C. Jun, X. M. H. Huang, M. Manolidis, C. A. Zorman, M. Mehregany, and J. Hone: Nanotechnology **17** (2006) 1506.
23) A. V. Grigorov and A. Boisen: Microelectron. Eng. **78–79** (2005) 190.
24) B. J. Gallacher, J. Hedley, J. S. Burdess, and A. J. Harris: Proc. Nanotechnology Conf. Trade Show, 2003, p. 478.
25) M. Chiao and L. Lin: J. Micromech. Microeng. **14** (2004) 1742.
26) R. R. A. Syms and D. F. Moore: Electron. Lett. **35** (1999) 1277.
27) S. Enderling, J. Hedley, L. Jiang, R. Cheung, C. Zorman, M. Mehregany, and A. J. Walton: J. Micromech. Microeng. **17** (2007) 213.
28) D. Joachim and L. Lin: J. Microelectromech. Syst. **12** (2003) 193.
29) C. G. Courcimault and M. G. Allen: Proc. 13th Int. Conf. Solid-State Sensors, Actuators and Microsystems, 2005, p. 875.
30) K. Tanaka, Y. Mochida, M. Sugimoto, K. Moriya, T. Hasegawa, K. Atsuchi, and K. Ohwada: Sens. Actuators A **50** (1995) 111.
31) J. C. Chiou and Y. J. Lin: J. Micromech. Microeng. **15** (2005) 1641.
32) R. D. Blevins: *Formulas for Natural Frequency and Mode Shape* (Krieger, Malabar, FL, 1984) p. 104.
33) T. C. Chang and R. R. Craig, Jr.: J. Eng. Mech. Div. ASCE **95** (1969) 1027.
34) P. A. A. Laura, J. L. Pombo, and E. A. Susemihl: J. Sound Vib. **37** (1974) 161.
35) D. Young and R. P. Felgar: Engineering Research Series No. 44, Bureau of Engineering Research, Austin, TX, 1949 [http://repositories.lib.utexas.edu/handle/2152/6001].
36) J. M. Gere and S. P. Timoshenko: *Mechanics of Materials* (PWS, Boston, MA, 1990) 3rd ed., p. 301.
37) National Applied Research Laboratories, National Chip Implementation Center, Hsinchu Science Park, Taiwan, R.O.C. [http://www.cic.org.tw].
38) The CIC CMOS MEMS Design Platform for Heterogeneous Integration, Chip Implementation Center, Taiwan, 2008 Document No. CIC-CID-RD-08-01.